Photoreceptor-Specific Temporal Contrast Sensitivities in RP1L1-Associated Occult Macular Dystrophy

Cord Huchzermeyer,[1] Julien Fars,[1] Jan Kremers,[1] Laura Kühlewein,[2] Melanie Kempf,[2] Saskia Ott,[2] Krunoslav Stingl,[2] and Katarina Stingl[2]

[1]Department of Ophthalmology, University Hospital Erlangen, Friedrich-Alexander-University Erlangen-Nürnberg, Erlangen, Germany
[2]Center for Ophthalmology, University Hospital Tübingen, Tübingen, Germany

Correspondence: Cord Huchzermeyer, University Eye Hospital, Schwabachanlage 6, Erlangen 91058, Germany; huchzi@email.de.

Received: December 23, 2022
Accepted: May 22, 2023
Published: June 21, 2023

Citation: Huchzermeyer C, Fars J, Kremers J, et al. Photoreceptor-specific temporal contrast sensitivities in RP1L1-associated occult macular dystrophy. *Invest Ophthalmol Vis Sci.* 2023;64(7):33. https://doi.org/10.1167/iovs.64.7.33

Purpose. The purpose of this study was to compare L-, M-, S-cone-, and rod-driven temporal contrast sensitivities (tCS) in patients with RP1L1-associated autosomal-dominant occult macular dystrophy (OMD), and to investigate how photoreceptor degeneration determines which post-receptoral channels dominate perception.

Methods. Photoreceptor isolating stimuli were created with the silent substitution technique. Photoreceptor-selective tCS deviations ($D_{L\text{-cone/M-cone/S-cone/Rod}}$) were obtained as a function of temporal frequency with identical retinal adaptation, by subtracting tCS from age-corrected normal values. A linear-mixed effects model was used for analysis.

Results. Eleven genetically confirmed patients were included (7 women, 5 men; age = 52.27 ± 14.44 years). Overall, L- and M-cone-driven sensitivity deviations ($D_{L\text{-cone}}$ and $D_{M\text{-cone}}$) were more negative than $D_{S\text{-cone}}$; D_{Rod} was normal at frequencies between 8 and 12 Hz in all subjects. Rod-driven tCS functions allowed identification of two subgroups of patients: one with band-pass properties and one with low-pass properties, suggesting dominance of different post-receptoral filters. The same filtering properties were observed in L-cone-driven tCS functions. Furthermore, the two subgroups also differed in clinical parameters (spherical equivalent, BCVA, perimetry, and ocular coherence tomography (OCT) reflectivity of the ellipsoid zone relative to the RPE).

Conclusions. OMD was characterized predominantly by deterioration of L- and M-cone-cone driven function in the perifovea. Rod-driven functions were normal. Differences in the photoreceptor signals were further modified by postreceptoral filters.

Keywords: occult macular dystrophy (OMD), silent substitution, postreceptoral pathways, temporal contrast sensitivity (tCS), chromatic pupil campimetry

Autosomal-dominant occult macular dystrophy (OMD) is a macular dystrophy characterized by the absence of visible funduscopic changes. Patients have impaired color discrimination[1,2] and display perimetric scotomas.[3] Optic coherence tomography (OCT) shows subtle alterations of the outer retina (loss of interdigitation zone [IZ]; blurring or discontinuity of the ellipsoid zone [EZ] in the macula; and loss of the dome-shaped configuration of the foveola),[4–6] and focal or multifocal electroretinograms show reduced responses in the macula.[7]

Frequently, it is caused by variants in the retinitis-pigmentosa1-like-1 (RP1L1) gene (OMIM #613587).[8,9] RP1L1 encodes for a protein that is part of the photoreceptor axoneme.[10,11] It is expressed in both rods and cones, but large differences in phenotypes between different mutations suggest that it may play distinct roles in these photoreceptor types.[9] Whereas loss-of-function mutations cause retinitis pigmentosa with a predominant affection of rod function,[12] OMD is typically caused by the R45W sequence variant or by mutations more downstream (between amino acids 1172 and 1258).[9] Currently, it is not known whether OMD also affects rods.

Despite the genetic homogeneity, several authors have identified phenotypic heterogeneity in disease severity,[13] in spatial involvement (central and paracentral; focal and widespread),[14] and/or in different types of scotomas (central scotoma, perifoveal scotoma, and no scotoma).[3] However, it is not clear whether different phenotypes are genuine or if they represent different stages in disease progression,[4] although severity is usually not correlated with age.[4,15]

Functional tests that enable a better characterization of the function of retinal cell types and pathways are likely to extend our knowledge about pathological mechanisms. The silent substitution technique is used for selective stimulation of different photoreceptor types in psychophysical and electrophysiological tests.[16,17] It is more reliable than chromatic adaption and allows the different photoreceptor types to be studied at the identical state of adaptation. Therefore, there are more degrees of freedom for creating stimulus conditions, and parameters like temporal frequency or contrast

can be used to investigate the influence of postreceptoral pathways on perception.[18]

In contrast to the chromatic desensitization technique, the silent substitution technique does not make the targeted photoreceptor more sensitive to a stimulus by altering retinal adaptation or using stimulus properties that favor one photoreceptor subtype. Instead, it aims to create stimuli that induces an excitation modulation in one photoreceptor type but not in the others (that are "silenced").[16,17,19] This is achieved by using several, usually three to five, primaries (i.e. spectrally independent light sources) with different spectral composition (ideally stimuli with small bandwidths) and knowledge about the spectral sensitivities of the photoreceptor types (the so-called fundamentals).[20]

Psychophysical thresholds for detection of photoreceptor-specific stimuli do not only depend on properties of the photoreceptor (mosaic density, temporal processing, etc.), but also properties of the postreceptoral channels. For example, thresholds for L- or M-cone-isolating stimuli are lower at low than at high temporal frequencies. Furthermore, in normal trichromats, L- and M-cone driven thresholds are equal at low temporal frequencies, whereas L-cone driven thresholds are generally smaller than M-cone driven thresholds at high temporal frequencies. These differences can be explained because the (parvocellular) red-green opponent system mediates detection thresholds at low temporal frequencies whereas the fast (magnocellular) luminance system is responsible for detection at high temporal frequencies. These effects can be studied by measuring temporal contrast sensitivity as a function of temporal frequency (tCS functions or de Lange curves).

The shape of these tCS function reflects the filtering properties of the postreceptoral retinogeniculate and central pathways. The red-green opponent system receives balanced and antagonistic inputs from the L-cones and M-cones and has low-pass-shaped temporal properties (sensitivities are maximal at low temporal frequencies with a sharp decrease around 8 hertz [Hz]).[21,22] It is associated with a subjective perception of a red-green color change.[21] The magnocellular luminance system, on the other hand, receives L- and M-cone signals that reinforce each other and that are L-cone dominated in most subjects with normal color vision (maximal sensitivity at an intermediate frequency)[21,22] and is associated with the perception luminance modulation or flicker.[21] The temporal contrast sensitivity functions for L- or M-cone-isolating stimuli result from a combination of both types of pathways.[21,22] The koniocellular pathway compares S-cone inputs with combined L- and M-cone inputs. It also acts as a low-pass temporal filter. Finally, there are at least two different rod pathways: one where signals are passed on via rod-bipolars and horizontal cells, and one where signals are passed on via gap junctions to cones.[23] The first pathway has band-pass properties with a maximal sensitivity around 8 to 12 Hz. The signals that are fed into the second pathway are passed on via parvo- and magnocellular systems.[24,25]

The importance of postreceptoral processing of retinal signals for functional tests is widely underestimated. Whereas most clinicians understand that functional losses originate at different levels of the visual pathway, they implicitly assume that postreceptoral processing is unaltered in diseases of the outer retina. However, findings, such as increased thickness of the inner retina in patients with RPGR,[26] indicate that even the cellular substrate of postreceptoral processing may indeed be altered. Furthermore, postreceptoral pathways act as filters on photoreceptoral signals, and alterations purely at the photoreceptor level may determine which postreceptoral channel mediates visual perception. Thus, complex changes in sensitivity may occur when distinct postreceptoral pathways mediate perception under different stimulus and adaptation conditions.

We previously used an LED stimulator[27] with a circular perifoveal test field with 2 degrees inner and 12 degrees outer diameter to measure changes in photoreceptor-specific temporal contrast sensitivities in patients with retinitis pigmentosa (RP)[28] and with Fundus flavimaculatus/Stargardt's disease (FF/STGD).[29] In both diseases, we found no clear indication of changes in post-receptoral mechanisms, and we found a predominant rod-driven loss in RP and similar losses across all photoreceptor subtypes in FF/STGD.

It is the purpose of the present study to measure perifoveal photoreceptor-specific tCS functions in patients with OMD. The results of these measurements enable (1) a comparison of functional losses in distinct photoreceptor subtypes and (2) a description of the involvement of postreceptoral pathways in OMD.

Methods

In this observational, cross-sectional pilot study, we measured L-cone, M-cone, S-cone-, and rod-driven temporal contrast sensitivities (tCSs) in patients with genetically confirmed autosomal-dominant OMD caused by mutations in the Retinitis-pigmentosa-1-like-1 gene (RP1L1). The method was combined with chromatic pupil campimetry, OCT, and adaptive optics imaging in some patients. Patients were recruited from the Inherited Retinal Diseases (IRD) clinics of the University Eye Hospitals Tübingen and Erlangen between May 2021 and January 2022, and data from one patient who was examined in April 2013 was included in the dataset. We pursued a study size of 10 patients, based on our experience with similar studies in patients with RP[28] and STGD,[29] taking into consideration that OMD is a rare disease. For each patient, all measurements were performed during a single visit.

Patients with concurrent retinal disease, medication known to affect retinal function, and/or conditions preventing participation in psychophysical tests, like dementia and Parkinson's disease, were excluded.

The study adhered to the tenets of the Declaration of Helsinki and was approved by the ethics committee of the Medical Faculty of the Friedrich-Alexander-University Erlangen-Nürnberg (300-17B) and the ethics committee of the Medical Faculty of the University of Tübingen. Patients gave written informed consent prior to inclusion in the study. All patients underwent a basic ophthalmological examination with objective and subjective refraction, best-corrected visual acuity, perimetry, color vision tests, and funduscopy.

Perimetry

Standard-automated perimetry of the central 10 degrees (M-pattern) was performed using a Haag-Streit Octopus 900 perimeter (Haag-Streit, Köniz, Switzerland). Data were exported as a CSV file and further analyzed using the visualFields package[30] for the statistical programming language R.[31]

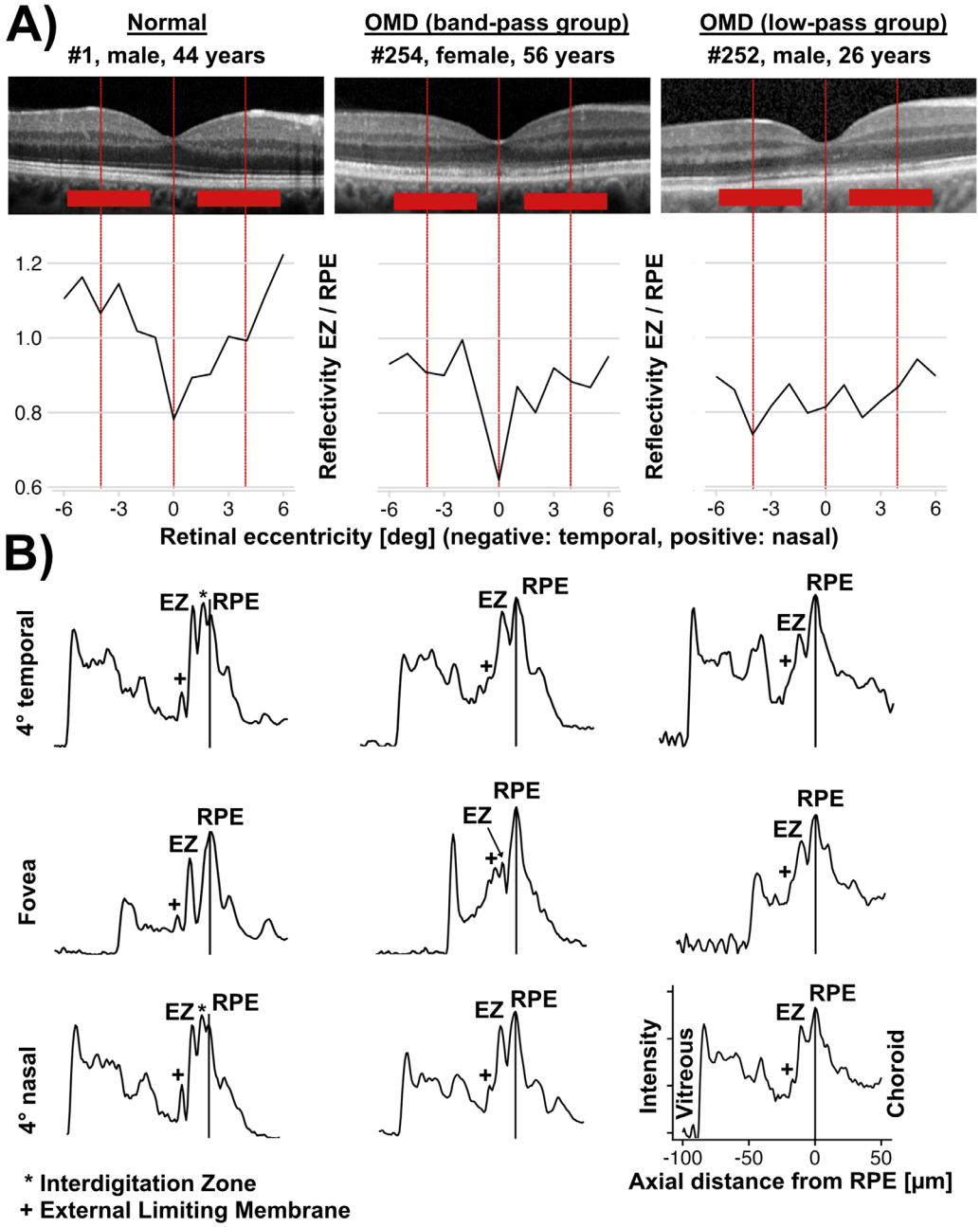

Figure 1. Analysis of OCT reflectivity profiles. Thirteen regions of interest (ROIs) were placed, one in the foveola and six on each side with 100 µm distance (in emmetropic eyes, these ROIs correspond to retinal eccentricities between 0 degrees and 6 degrees). Panel (**A**) shows OCTs of three subjects (one normal subject, one patient from band-pass group, and one from low-pass group) and the location of three ROIs (vertical dashes lines in panel **A**: 0 degrees, 4 degrees nasally, and 4 degrees temporally). The horizontal red bars in the OCT images indicate the spatial configuration of the LED stimulator's test field. Within these ROIs, reflectivities of the ellipsoid zone and the retinal pigment epithelium were measured (see Panel **B**, scaling shown in the *lower right corner*), and the EZ reflectivity was normalized to the RPE reflectivity within each ROI, resulting in the curves in the lower half of panel **A**.

Ocular Coherence Tomography

Spectral-domain OCT scans of the macula centered on the fixation locus (at least one horizontal and one vertical) were obtained with the Heidelberg Retina Analyzer (HRA; Heidelberg Engineering, Heidelberg, Germany). A horizontal section was exported as a TIF file, cropped, and converted to grayscale using the GNU Image Manipulation Program (version 2.10.14; The GIMP Development Team, https://gimp.org), and further analyzed using the OCT Reflectivity Analytics (ORA) software.[32] Details of the analyses of OCT reflectivity profiles are shown in Figure 1.

Color Vision Tests

At least one of the following color vision tests was performed monocularly in each subject: anomaloscope (Rayleigh equation), Panel-D15, or Cambridge Color Test. An HMC

anomaloscope (Oculus, Wetzlar, Germany) was used to characterize red-green color matches with the Rayleigh equation. The red-green ratio in the test field was adjusted by the experimenter while the observer adjusted the brightness of the reference field. Although the anomaloscope is the gold standard for identifying X-chromosomal color vision defects, it is often difficult to perform measurements in patients with OMD with a loss in central vision due to the small test field.

The (saturated) Panel D15 was performed under standardized lighting conditions. After thorough instructions, subjects ordered the caps according to hue. Quantitative scoring was performed according to the method by Vingrys and King-Smith,[33] with the C-index (confusion index), the S-index (selectivity index), and confusion angle used as outcome parameters. X-chromosomal color vision defects were suspected when the S-index was high, and the angle was compatible with confusion along the protan or tritan axis.

The Cambridge Color Test (CCT) uses computer-generated pseudoisochromatic patterns that are presented on a self-calibrating, gamma-corrected 32 inch LCD screen with 1920 × 1080-pixel resolution (display++ monitor) to test color discrimination along the three major axes (trivector version of the CCT). The hardware is part of the Metropsis Visual Function Assessment System (Cambridge Research Systems, Cambridge, UK). The test field depicts a Landolt-C with an opening in one of four directions (four-alternative-forced choice test). X-chromosomal defects were suspected when discrimination along the tritan axis was significantly better than defects along the deutan- and protan-axes. The latter are always highly correlated.

Photoreceptor-Specific Temporal Contrast Sensitivities

Temporal contrast sensitivity quantifies the ability to detect temporal modulation. In the present study, modulation was presented around a white background (CIE coordinates x = 0.38, y = 0.28; retinal illuminance 289 photopic trolands [phot Td]) that was a combination of the output of four colored LEDs (red, green, blue, and cyan). The output of these four LEDs was modulated such that the excitation of only one of the four photoreceptor types was also modulated, whereas the excitation of the remaining photoreceptor types was constant. The observer was asked to indicate if a change in luminance and/or in hue could be perceived.

Apparatus. The dedicated four-primary LED stimulator that we used to measure temporal contrast sensitivities has been described in detail by Pokorny et al.[27] This apparatus has two major advantages. First, the stimulus consists of four colors with small spectral bandwidths allowing isolation of the response of one photoreceptor type with reasonable contrast. Second, modulation of the stimulus can be obtained with a very high temporal resolution (2 kHz). However, the stimuli are spatially fixed.

Briefly, the stimulus is created by combining the output of four differently colored LEDs (peak intensities at 660 nm, 558 nm, 516 nm, and 460 nm) for each of 2 test fields: a central circular field with 2 degrees diameter and a surrounding annular field with 2 degrees inner and 12 degrees outer diameter. The LEDs' spectral bandwidths at half-height are reduced to approximately 8 to 10 nm by means of interference filters. The apparatus uses a Maxwellian view optical pathway, where the images of the LEDs are projected onto the pupil to maximize retinal illuminance. The luminance of each LED is controlled with high temporal resolution (2 kHz) by one of eight channels of the soundcard of a personal computer and a digital analogous converter that converts the soundcard's amplitude-modulated output into a frequency-modulated signal that drives the LEDs.[34]

Spatial, Temporal, and Spectral Properties of the Stimuli. We used the outer annular stimulus as the test field for obtaining photoreceptor-specific temporal contrast sensitivities in the perifovea. Testing the perifoveal region was chosen to decrease the interindividual variability caused by individual differences in the macular pigment optical density.

The LEDs were modulated sinusoidally, either in phase or in counter-phase. This phase and the temporal contrasts were chosen in a way that the changes in the number of photoisomerizations caused by each LED were zero in all except one photoreceptor type (triple silent substitution). In this manner, four stimulus conditions with selective stimulation of L-cones, M-cones, S-cones, and rods were created. The excitation contrasts in the targeted photoreceptor types were varied by varying LED contrasts while keeping their contrast ratios and phases constant. The contrasts were calculated based on the LED spectra and the spectral sensitivities of the photoreceptor types (cone fundamentals). The procedure and its validation in dichromats are described in more detail elsewhere.[21,35]

Measurement Protocols. Measurements were carried out at mesopic light levels (289 phot Td) in a dimly lit room after adaption to these ambient conditions for at least 5 minutes. Temporal contrast sensitivity was measured using a yes/no-forced choice randomly interleaved double staircase algorithm – one staircase starting at zero, the other at maximal contrast – with temporal frequencies of 1, 2, 4, 6, 8, 10, 12, 16, and 20 Hz. The subjects were instructed to fixate within the 2 degrees outer diameter central field, which has half the illuminance as the annular test field.

Photoreceptor-Specific Temporal Contrast Sensitivity. We used the triple silent substitution technique to create stimuli to modulate the excitation selectively in one class of photoreceptors and to measure detection thresholds. The thresholds are not only determined by the properties of the photoreceptors themselves but also by the post-receptoral pathways that mediate perception (L+M, L-M, or both). Therefore, temporal contrast sensitivity to L-cone-isolating stimuli should be called L-cone-*driven* tCS, and we used this throughout the manuscript. We used the term *photoreceptor-specific* tCS only as a generic term for a tCS driven by a not-specified single photoreceptor type subtype.

Photoreceptor-specific tCS is expressed in decibels, calculated according to Equation 1.

$$S[dB] = 10 \times log_{10} \frac{100\%}{C_{threshold}}$$

Consequently, a sensitivity of 0 dB corresponds to thresholds of 100% Michelson contrast. However, it is not technically possible to achieve 100% contrast at the photoreceptor level. With our settings, the maximal contrast at the photoreceptor level was 25% for L-cones, 23% for M-cones, 83% for S-cones, and 27% for rods (expressed in terms of Michelson cone or rod contrast), resulting in minimal measurable sensitivities of 6.03 dB, 6.33 dB, 0.82 dB, and 5.64 dB,

respectively. When observers were unable to perceive modulation at the maximal technically possible contrast, we use the minimal sensitivities as a conservative estimate for calculations (floor effect).

Calculating sensitivity deviations facilitates comparison between different photoreceptor types and frequencies. The (sensitivity) deviation, D, for each photoreceptor type (dB) is defined in Equation 2.

$$D\,[dB] = S_{observed} - S_{normal,40years} + (Age - 40\ years) \times\ 0.1\frac{dB}{year}$$

Where $S_{observed}$ is the measured sensitivity; $S_{normal,\ 40\ years}$ is the measured sensitivity in a 40-year-old heathy subject obtained from previous measurements; and age is the age of the patient. The age-corrected normal values for a 40-year-old observer and the change of 0.1 dB/year were obtained from previous measurements with healthy subjects,[28] but we converted the published normative values to decibel and used the mean instead of the median. In the previous publication, we also showed data that justifies an identical linear age-correction across photoreceptor types and temporal frequencies.

Data Analysis

Outcome Variables. Primary outcome variables were the photoreceptor-driven temporal contrast sensitivity deviations in comparison with normal values ($D_{\text{L-cone}}$, $D_{\text{M-cone}}$, $D_{\text{S-cone}}$, and D_{Rod}). We tested for systematic differences between photoreceptor types using a linear mixed-effects model.

During the study, we identified two different subgroups of patients who displayed distinct rod-driven tCS (see Results section). The so-called "band-pass group" displayed lower sensitivities at low temporal frequencies compared with sensitivities at higher temporal frequencies. The "low-pass" group showed similar sensitivities at low and high temporal frequencies. We used a more complex linear mixed-effects model to describe the differences between the subgroups. Furthermore, we tested for statistical differences between these groups in the secondary outcome variables: age, spherical equivalent, logMAR, perimetry, and OCT.

Statistical Testing. Linear mixed effects models were constructed for comparison of temporal contrast sensitivity deviations between photoreceptor types and for analyzing differences between two subgroups that were observed in the tCS deviation functions.

Photoreceptor type was modeled as a fixed factor, whereas individual patients were modeled as a random factor. Interactions between random and fixed effects were not included in the model, because we were interested in disease-specific (fixed) effects. The data were fit by the model using a restricted maximum likelihood estimation (REML) with the lmerTest package[36] for the R statistical software.[31]

A first model was used for statistical inference about differences in photoreceptor-specific tCS loss between photoreceptor types. Therefore, it only included photoreceptor type and patient, thus assuming disease-specific fixed differences between photoreceptor types and random differences in overall sensitivities between patients, but no effects of temporal frequency.

$$\mathrm{D_{i,j}\,[dB]} = \mu + \alpha_{\mathrm{i}} + \mathrm{u_j} + I \quad (1)$$

where μ is the intercept (see below), α_{i} is the fixed photoreceptor-related change (i refers to the photoreceptor type), $\mathrm{u_j}$ is the patient (j) related random variation ($\mathrm{u} \sim \mathrm{N}(0, \sigma_{\mathrm{j}}^2)$), and $\in_{\mathrm{i,j}}$ is the remaining error ($\in \sim \mathrm{N}(0, \sigma_{\mathrm{i,j}}^{\mathrm{I}})$). We chose this model, because linear mixed-effects models allow to draw conclusions about the population (i.e. all patients with OMD) from which the study cohort was sampled while taking into consideration the intra-observer lack of independence between the photoreceptor types.[37]

Because the conclusions drawn from this first model are paramount to our study and because statistical inference from linear mixed effects may not always be reliable, we also used an alternative model for analyzing disease-specific fixed effects while accounting for intra-individual variability in overall sensitivities based on analysis of variance (ANOVA).

Furthermore, we fitted a second model to the data that also incorporated differences between two different subgroups of patients that could be distinguished based on the rod tCS deviation functions (see Results section).

This model is descriptive, because it compares the same parameters between two subgroups that were initially used to subdivide patients. The model therefore does not provide evidence for the validity of the subdivision. Instead, we used the Wilcoxon test, the *t*-test (both after Holms correction for multiple testing) and the ANOVA (as appropriate) on the following parameters to make inferences on the external validity of the subdivision: age, BCVA, spherical equivalent, perimetric defect, OCT, and EZ/RPE reflectivity ratio.

In the "bandpass" subgroup, the functions displayed lower sensitivities at low temporal frequencies and a sensitivity maximum around 8 to 12 Hz. In the "low pass" subgroup, the sensitivities were high at low temporal frequencies and only decreased at high temporal frequencies. In this second linear mixed-effects model, we used only the frequency range between 8 and 12 Hz and included interactions between patient subgroup and photoreceptor types.

$$D_{i,j}\,[dB] = \mu + \alpha_i + \beta_j + \alpha\beta_{i,j} + u_k + \in_{i,j} \quad (2)$$

where α_i is the fixed photoreceptor-related effect, β_j is the fixed effect of the groups, $\alpha\beta_{i,j}$ is the interaction between photoreceptor type and subgroup, and u_k is the patient-related random variation ($u \sim N(0, \sigma_j^2)$).

In both models, we used a "treatment model" parameterization, where an intercept μ corresponds to the L-cone-driven sensitivity in model 1 and to the L-cone-driven sensitivity in the low-pass group in model 2. This parameter is tested against zero ($\mathrm{H_0}$: μ = 0). The other parameters are tested against this intercept (for example, $\mathrm{H_0}$: $\alpha_{Rod} - \mu = 0$). If a "cell means model" was used instead, all photoreceptors would be tested against 0 and direct statistical comparison between photoreceptors would not be possible.

Results

Patient characteristics are reported in Table 1. Eleven patients (7 women and 4 men) were included in this cross-sectional observatory study (age = 52.27 ± 14.44 years and 26 to 71 years). Patients had reduced visual acuities (logMAR = 0.936 ± 0.511, between 0.49 and 1.3, corre-

Table 1. Patient Characteristics

	Age	Sex	Eye	Mutations	SE (D)	logMAR	MD (dB)	CFT (µm)
37	67	F	OD	RP1L1: R45W	+0.62	0.80	5.10	154
245	43	F	OD	RP1L1: R45W	−10.00	1.00	5.90	256
246	45	M	OD	RP1L1: R45W	−2.12	0.70	6.45	155
247	71	F	OD	RP1L1: R45W	+1.00	1.30	6.90	189
248	66	M	OD	RP1L1: R45W	−3.75	1.00	6.79	168
249	33	F	OD	RP1L1: R45W	0.00	0.60	2.07	176
250	52	M	OS	RP1L1: R45W	−1.13	0.60	8.25	197
251	53	F	OD	RP1L1: R45W	−0.25	0.49	6.90	183
252	26	M	OD	RP1L1: R45W	−3.75	0.90	5.10	186
253	63	F	OD	RP1L1: R45W	−7.62	1.30	7.80	158
254	56	F	OD	RP1L1: R45W	+1.50	0.60	6.80	196

SE, spherical equivalent; MD, mean defect (10 degrees standard-automatized perimetry); CFT, central foveal thickness (OCT).

sponding Snellen acuities of 0.32 and 0.05, respectively) and perimetric losses in the central 10 degrees visual field (mean defect = 6.3 ± 0.99 dB). No patient had undergone cataract surgery, although one patient (#247) had clinically relevant cataract. Patients #251 and #253 took dietary supplements. Six patients were myopic (spherical equivalent < −1 dpt).

All subjects underwent at least one color vision test (CCT: $n = 7$, Anomaloscope: $n = 6$, and Panel-D15: $n = 9$). The results are shown in Table 2: almost all subjects had impaired color discrimination, (only subject #252 had a normal discrimination CCT threshold along the tritan axis and thresholds close to normal along the protan- and deutan-axes, small AQ range, and normal Farnsworth D15). One other patient (#245) also had a normal Farnsworth D15 (C-index of 1.00), but the same patient had markedly elevated color discrimination thresholds in the CCT. Thus, even minor transpositional errors in the D15 panel as were observed, for example, in patient #249 indicate relevant dyschromatopsia.

Two patients had very large matching ranges in the anomaloscope examination (Rayleigh equation). In patient #37 (a female patient), the range included 1 and the color discrimination in the CCT was at instrument gamut, indicative of a severely disrupted color discrimination. In the other patient (#246, a male patient), the midpoint was shifted toward green, but the examination was very difficult for this patient. In the CCT, he had protan and deutan discrimination thresholds close to gamut (protan 102 and deutan 101), whereas tritan discrimination was relatively preserved (56). Furthermore, the L- and M-cone-driven temporal contrast sensitivities ($S_{L\text{-cone}}$ and S_{Rod}) at low temporal frequencies were suggestive of protanopy (see below). However, a Farnsworth D15 color vision test from 2014 (and therefore not shown in Table 2) argued against congenital dichromacy. A third patient, #253 (a female patient) also had very high color discrimination thresholds in the CCT.

Patient #250 had relatively selective confusion lines in the Panel-D15 test, with an angle that indicated possible protanomaly. No other color vision tests were performed in this patient.

Temporal Contrast Sensitivities

Temporal contrast sensitivities ($S_{L\text{-cone}}$, $S_{M\text{-cone}}$, $S_{S\text{-cone}}$, and S_{Rod}) of the 11 patients are shown in Figure 2, ordered by photoreceptor type and decade of age. Sensitivities were mostly below age-corrected normal values but sometimes not outside the mean ± SD range (shown in Fig. 2). As in healthy subjects, sensitivities often had low-pass characteristics.

One patient (#246, a 45-year-old man) had severely impaired L-cone-driven sensitivities ($S_{L\text{-cone}}$) across all frequencies. This patient also showed reduced $S_{M\text{-cone}}$ at low temporal frequencies but not at high temporal frequencies. A similar pattern is found in patients with X-chromosomal protanopy, in agreement with the results of the examinations with the anomaloscope and the CCT (see above). However, the results of a Panel-D15 test that was performed years before (in 2014) argued against that possibility.

The oldest patient (#247, a 71-year-old woman) with manifest cataract had severely impaired S-cone-driven sensitivities $S_{S\text{-cone}}$, whereas S-cone-driven sensitivities were normal in most other subjects. This patient also had severely impaired S_{Rod} values that could not be measured, because

Table 2. Color Vision Tests

	Cambridge Color Test (CCT)			Anomaloscope		Saturated Farnsworth D15 Test			
ID	Protan	Deutan	Tritan	AQ_{mean}	AQ_{range}	S-Index	C-Index	Angle [°]	Comment
37	110.0*	110.0*	110.0*	5.47	10.20*	1.15	1.19	−70.15	Large anomaloscope matching range; poor discrimination in CCT
245	74.4	54.7	13.8	1.16	0.68	1.38	1.00	61.98	
246	102.1*	100.7*	55.6*	13.27	15.21*				Very large anomaloscope matching range; poor Protan and Deutan discrimination in CCT
247						only non-saturated Panel-D15			
248						1.30	2.04	3.45	
249						1.18	1.35	−45.22	
250						2.58*	2.70*	3.14*	D15: high selectivity index
251	43.2	36.6	28.2			1.30	1.82	−15.61	
252	16.5	11.4	10.5	0.72	0.00	1.38	1.00	61.98	
253	110.0*	110.0*	89.1*	1.52	1.91	1.79	1.31	57.83	Poor discrimination in CCT
254	25.1	35.0	16.7	1.04	0.63	1.29	1.23	−3.62	
NV	*<10*	*<10*	*<15*	*1.0 ± 0.2*	*4.4 ± 3.8*	*1.38*	*1.00*	*+61.98*	

Patients 37, 246, 250, and 253 had very poor results in one of the color vision tests, as indicated by the asterisks. Patient #246 also had a pattern of photoreceptor-specific temporal contrast sensitivity loss suggestive of protanopy. The last line (NV) indicates the normal values for the Cambridge Color Test (CCT),[38] the HCM anomaloscope,[39] and the saturated Panel-D15.[33]

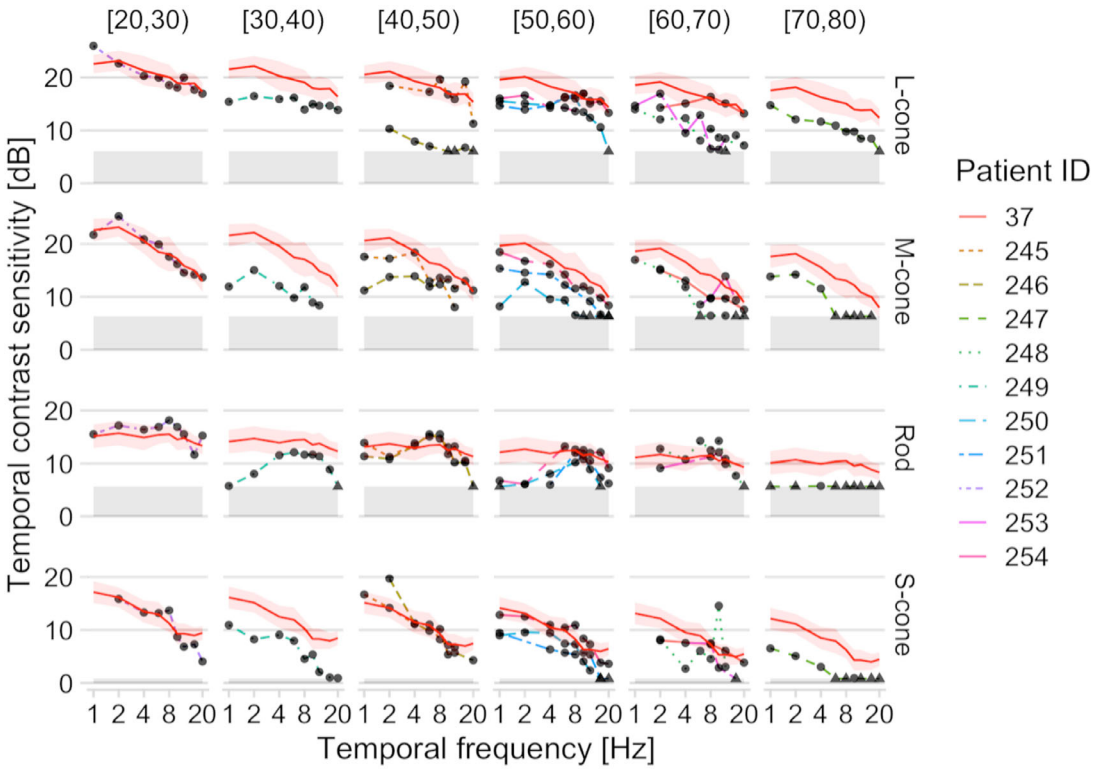

Figure 2. Temporal contrast sensitivities, shown separately for different age groups (decade) and photoreceptor types. The *red line* shows the age-corrected normal sensitivity, and the *red area* shows the normal range ±1 SD.[28] The gray area at the bottom shows the sensitivities that could not be measured because they were beyond the instrument's gamut. When subjects were not able to see the maximal technically possible contrast, we used the gamut as a conservative estimate of sensitivity. Note that S-cone- and rod-driven sensitivities were often within the normal range, and even L- and M-cone-driven sensitivities were not always reduced. The oldest patient (#247) had very poor S-cone- and rod-driven sensitivities, possibly due to the presence of cataract. One patient (#246) has very poor L-cone-driven-sensitivities and reduced M-cone-driven sensitivities at low temporal frequencies.

the gamut of the stimulator was reached (dynamic range is very limited for rods in this age cohort).

The youngest subject (#252, a 26-year-old man), on the other hand, had basically normal temporal contrast sensitivities for stimulation of all photoreceptor types.

In a subgroup of patients (37, 249, 250, 251, and 254), rod-driven (and L-cone-driven) sensitivities were impaired at low, but not at high temporal frequencies (i.e. showing band-pass characteristics [around 12 Hz], rod-driven sensitivities were normal in almost all subjects). This group was designated as the "band-pass group." This was not observed in the other patients. Later, we will show how these subgroups differ by comparing analyzing temporal contrast sensitivity deviations and clinical parameters.

Overall Differences Between Photoreceptor Types

Overall differences in temporal contrast sensitivity deviation ($D_{L\text{-cone}}$, $D_{M\text{-cone}}$, $D_{S\text{-cone}}$, and D_{Rod}) among photoreceptor types were analyzed with the first linear mixed-effect model detailed in the Methods section. This model demonstrated an L-cone-driven sensitivity defect $D_{L\text{-cone}}$ (corresponding to μ in Equation 1) of 4.00 dB ($p < 0.01$), a nonsignificantly larger M-cone-driven defect (difference $\alpha_{L\text{-cone}}$: −0.10 dB, $P = 0.8$), and significantly smaller S-cone- and rod-driven defects (differences $\alpha_{S\text{-cone}}$ of 1.66 dB with $p < 0.01$ and α_{Rod} of 2.32 dB with $p < 0.01$). An alternative model based on ANOVA corroborated these results (overall $p < 0.01$, L-cone-driven intercept of −3.1 dB and differences with this intercept of −0.05 dB for M-cones, 1.64 dB for S-cones, and 2.35 dB for rods).

Temporal Contrast Sensitivity Deviations in Two Subgroups

The tCS deviation functions are shown as a function of temporal frequency in Figure 3. The upper plots show the results for the patients belonging the band-pass group (reduced rod-driven sensitivities at low temporal frequencies). The lower plots show the results for the remaining patients who displayed low-pass characteristics. This group was thus designated as the "low-pass group" (similar rod-driven sensitivities at low and high temporal frequencies). Note that L-cone-driven (and also S-cone-driven) tCS deviation functions in the band-pass group had similar band-pass characteristics as the rod-driven functions (i.e. lower sensitivities at low temporal frequencies). The tCS deviations in the low-pass group were more heterogeneous than in the band-pass group.

The second linear-mixed effects model (Equation 2) detailed in the Methods section describes the tCS deviation in the frequency range between 8 Hz and 12 Hz whereas considering differences between the two subgroups. The interpretation that the parameters offer is detailed in Table 3. The model fits are shown in Figure 3 by the shaded areas.

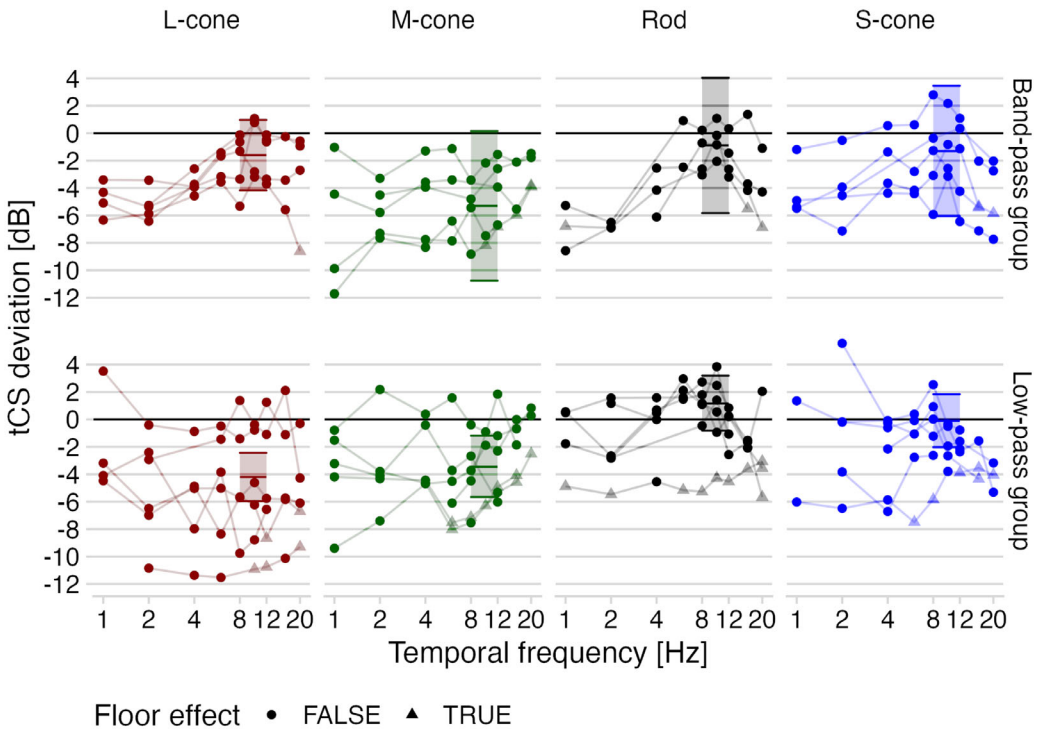

Figure 3. Temporal contrast sensitivity deviations (negative values indicate loss). These plots show the difference between the observed photoreceptor-specific contrast sensitivities and the age-related normal values as a function of temporal frequency. Patients were subdivided into two different groups according to the patterns in rod-driven tCS deviation (band-pass versus low-pass). The curves in the low-pass group (similar rod-driven tCS losses at low and at high frequencies) were more heterogeneous and there was more variability between neighboring frequencies. In contrast, the curves in the band-pass group (selective loss in rod- and L-cone-driven tCS at low frequencies) were much more homogeneous. The bars indicate the parameter estimates of a linear mixed-effects model (parameter estimate and 2.5/97.5 confidence intervals) that was fitted to the frequency range of 8 to 12 Hz. Patients in the band-pass group had a pronounced M-cone-driven tCS deviation, whereas patients in the low-pass group had similar losses in L- and M-cone-driven sensitivities.

Table 3. Calculation of The Photoreceptor-Specific Deviations From The Parameters of The Linear Mixed-Effect Model #2, Along With The Interpretation of The Different Parameters

D	Group	Parameter	Interpretation
L-cone	low-pass	$\boldsymbol{\mu}$	Is $\mu/D_{L\text{-cone}}$ different from 0?
M-cone		$\mu + \boldsymbol{\alpha_{M-cone}}$	Do $D_{M\text{-cone}}$, $D_{S\text{-cone}}$ and D_{Rod} differ from $D_{L\text{-cone}}$?
S-cone		$\mu + \boldsymbol{\alpha_{S-cone}}$	
Rod		$\mu + \boldsymbol{\alpha_{Rod}}$	
L-cone	Band-pass	$\mu + \boldsymbol{\beta_{band-pass}}$	Is $D_{L\text{-cone}}$ different between the two groups?
M-cone		$(\mu + \beta_{band-pass}) + (\alpha_{M-cone} + \boldsymbol{\alpha\beta_{band-pass,\,M-cone}})$	Are the photoreceptor effects different between the two groups?
S-cone		$(\mu + \beta_{band-pass}) + (\alpha_{S-cone} + \boldsymbol{\alpha\beta_{band-pass,\,S-cone}})$	
Rod		$(\mu + \beta_{band-pass}) + (\alpha_{Rod} + \boldsymbol{\alpha\beta_{band-pass,\,Rod}})$	

The interpretation refers to the parameters printed in bold.

L-cone driven tCS deviation ($D_{L\text{-cone}}$) in the low-pass group served as reference and was significantly different from zero (μ: −4.2 dB, $P < 0.001$), and $D_{L\text{-cone}}$ deviation tended to be less negative in the band-pass group (difference $\beta_{band-pass} = +2.6$ dB, $P = 0.07$). $D_{M\text{-cone}}$ was not significantly different from the reference $D_{L\text{-cone}}$ in the low-pass group (slightly less deviation, $\alpha_{M-cone} = +0.7$ dB, $P = 0.53$), but $D_{M\text{-cone}}$ was significantly larger than $D_{L\text{-cone}}$ in the band-pass-group ($\alpha\beta_{band-pass,\,M-cone}$: −4.4 dB, $P = 0.01$). $D_{S\text{-cone}}$ and D_{Rod} were much smaller than $D_{L\text{-cone}}$ in the lowpass-group (α_{S-cone}: +4.1 dB, $P < 0.001$; α_{Rod}: +5.4 dB, $P < 0.001$). This was similar in the band-pass-group, but this difference between $D_{S\text{-cone}}$ and D_{rod} on the one hand and $D_{L\text{-cone}}$ on the other hand was significantly less pronounced ($\alpha_{S-cone} + \alpha\beta_{band-pass,\,S-cone}$: +0.3 dB, $P = 0.01$; $\alpha_{Rod} + \alpha\beta_{band-pass,\,Rod}$: +0.8 dB, $P = 0.004$).

Differences in Clinical Parameters Between Subgroups

There were no systematic differences in age between the two subgroups (51.0 ± 10.12 vs. 52.5 ± 16.4 years; $P = 0.8$ after adjustment for multiple testing; see Fig. 4A), but patients in the low-pass group had significantly poorer best-corrected visual acuities (logMAR of 1.03 ± 0.23 vs. 0.62 ± 0.11; $P = 0.04$ after adjustment for multiple testing; see Fig. 4B). Furthermore, there was a tendency for these patients to be more myopic than patients in the band-pass group (−4.38 ±

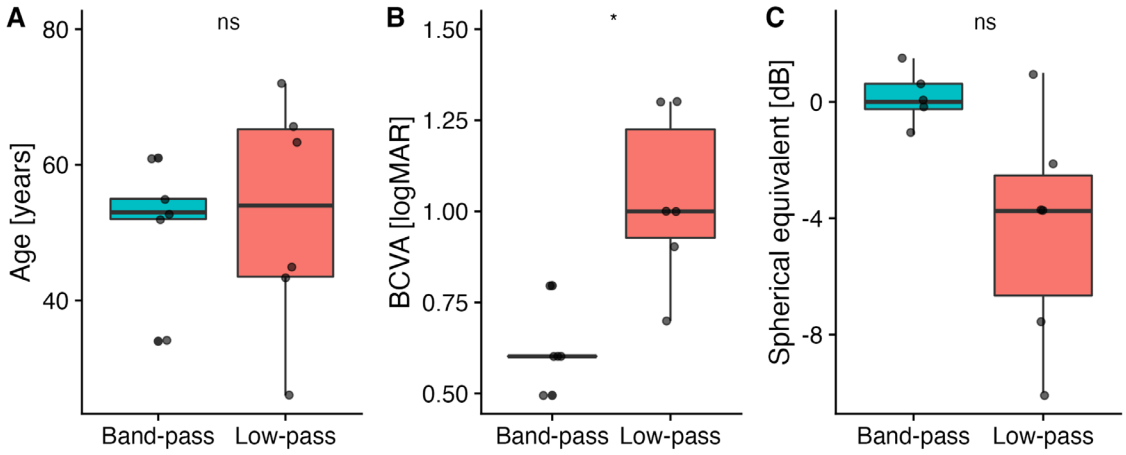

Figure 4. Age (*left*), best-corrected visual acuity (*middle*), and spherical equivalent (*right*). The comparison between both subgroups shows that patients with suppressed photoreceptor-specific temporal contrast sensitivities at low temporal frequencies (band-pass group) had significantly better best-corrected visual acuities and tended to be emmetropic rather than myopic. The exact *P* values are reported in the text.

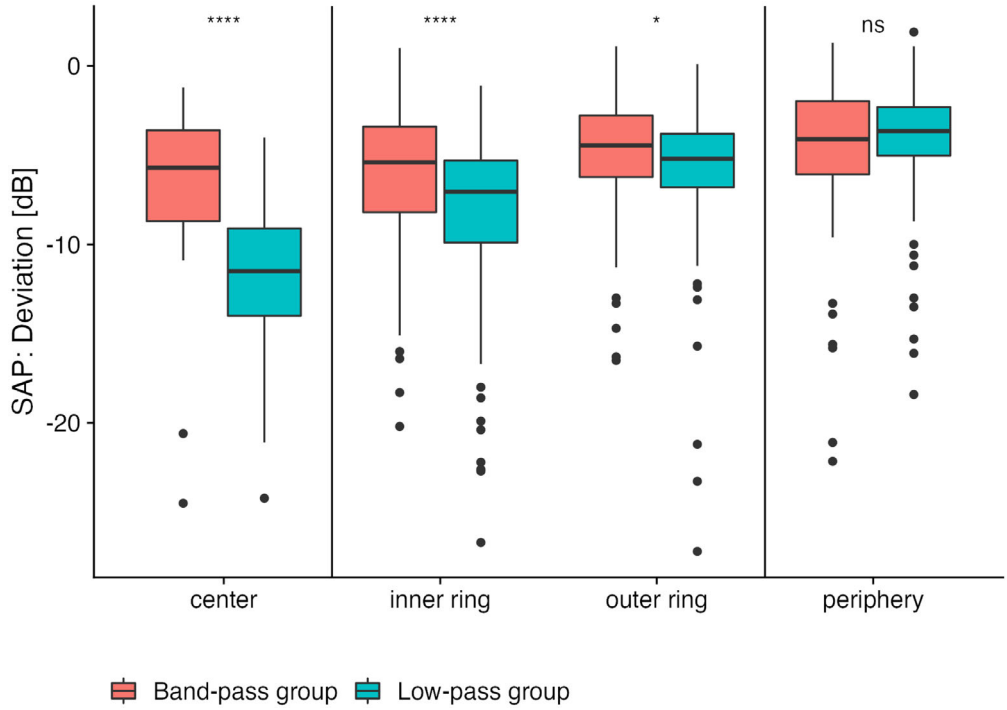

Figure 5. Perimetric sensitivity deviations in the central visual field. Deviation values were averaged in: (1) the central field (0 to 1 degrees retinal eccentricity), (2) the rings between 1 and 3.5 degrees eccentricity and between 3.5 and 6 degrees eccentricity, and (3) the periphery between 6 and 10 degrees retinal eccentricity. The rings correspond to the inner and the outer portion of the ring-shaped test field of the LED stimulator that was used to measure photoreceptor-specific tCS. The center is illuminated but not modulated by the stimulator, whereas the periphery is completely outside the test field.

3.92 vs. 0.15 ± 0.98 D; $P = 0.11$ after adjustment for multiple testing; see Fig. 4C). Patients in the band-pass group had also significantly poorer perimetric sensitivity in the center (Fig. 5).

OCT Differences Between Subgroups

The EZ reflectivity/RPE reflectivity ratio was significantly reduced in all patients in the perifoveal region, and these changes gradually merged into intact EZ toward the margins. Typical images are shown in Figure 1. A visible interdigitation zone was not present in any patient, but the external limiting membrane was largely intact in all patients. The results of the quantitative analysis are shown in Figure 6. Two subjects (#245 and #250 were excluded from analysis because of eccentric scan and poor image quality, respectively). In healthy subjects, the EZ/RPE reflectivity ratios were close to or above 1 in the perifovea, but there was

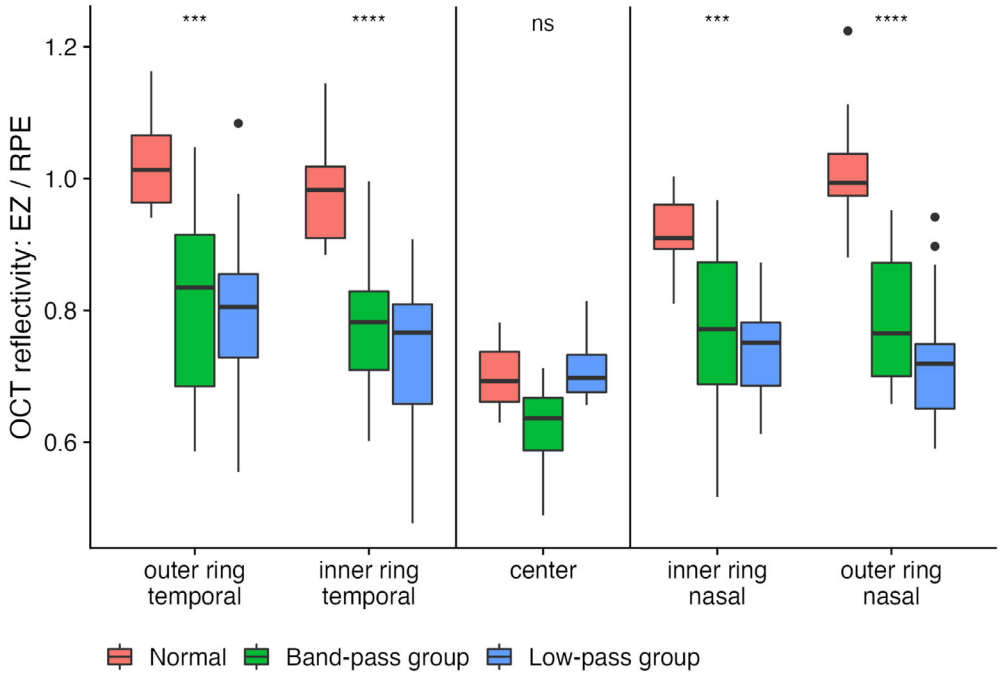

Figure 6. Reflectivity of the ellipsoid zone relative to RPE reflectivity at different retinal eccentricities. Data from patients #245 and #250 were excluded because of slightly eccentric scan in patient #245 and poor image qualitiy in patient #250. In the band-pass group, there is a clear trend ($P = 0.052$ after correction for multiple testing) toward a lower reflectivity in the fovea than in the perifovea. This group has relatively symmetric loss of reflectivity across the fovea, whereas patients in the low-pass group have lower reflectivity nasally (inner ring: 1 to 3 degrees eccentricity, and outer ring: 4 to 6 degrees eccentricity). The significances are calculated using ANOVA with Holm correction for multiple testing.

a clear drop in EZ reflectivity ratio in the fovea, possibly to the dome shape of the EZ in this area (see Fig. 1). Differences among all three groups (normal, band-pass, and low-pass) were statistically significant in the perifovea (caused by the large differences between healthy subjects and patients), but not in the fovea (see Fig. 6). Differences between patient groups were not statistically significant. The foveal decrease was also observed in patients in the band-pass group. The fact that overall loss of reflectivity was not smaller than in the low-pass group resulted in very low foveal reflectivity ratios in this group. However, the differences in the foveal reflectivity ratios were not statistically significant after correction for multiple testing (ANOVA; $P = 0.21$). The patients in the low-pass group did not show a drop in foveal reflectivity, but an asymmetry across the fovea with lower reflectivity ratios nasally than temporally was observed in several of these patients (see lower reflectivity ratios nasally in the low-pass group in Fig. 6).

In the qualitative analysis, OCT of the macula showed either blurring of the EZ (2/6 patients in low-pass group, and 4/5 in band-pass group), focal disruption of the EZ in the fovea (2/6 patients in low-pass group, and 0/5 in band-pas group). In the band-pass group, a hint of a dome-shaped EZ in the fovea was retained in two out of five patients.

In some patients, focal accumulation of hyper-reflective material extending from the retinal pigment epithelium to as far as the outer nuclear layer or retinal elevation anterior to a subretinal cleft were observed.

Discussion

This is the first description of photoreceptor-specific tCS deviation functions in patients with RP1L1-related occult macular dystrophy. The L- and M-cone-driven temporal contrast sensitivities were more severely impaired in the perifovea than S-cone-driven sensitivities.

Rod-driven sensitivities were almost normal, except for decreased sensitivities at low temporal frequencies in the band-pass group. This subgroup was characterized by an additional band-pass pattern in the L-cone-driven tCS deviation functions, a refraction close to emmetropia, relatively preserved best-corrected visual acuities, and a less pronounced decline in perimetric sensitivities toward the center of the visual field. This group had more homogeneous tCS functions, and tended to have more preserved foveal structure in the OCT.

In contrast, patients in the low-pass group had more heterogeneous tCS-deviation curves and more variability between adjacent frequencies ("noise"). Furthermore, these patients were more myopic, had poorer best-corrected visual acuities, and a more pronounced drop in perimetric sensitivities toward the center. Their OCT showed decreased EZ/RPE reflectivity ratios in the nasal region relative to the temporal region. Despite this clinically more severe phenotype, some of these patients had relatively preserved temporal contrast sensitivities.

The CCT allowed identification of acquired dyschromatopsia in patients with a normal D15 panel and can potentially be used as a sensitive test in OMD.[2] The saturated D15

panel, on the other hand, is known to have a low sensitivity, and, for example, a relevant number of deuteranomalous observers have normal results.[40]

Differences Between Photoreceptor Types

We found a predominant loss of L- and M-cone-driven tCS (shown by $D_{L\text{-cone}}$ and $D_{M\text{-cone}}$ values that strongly differ from 0). This seems to contrast with many other macular diseases, where a loss of S-cone-driven function dominates, most likely due to the relative sparsity and the limited dynamic range of the S-cones.[41] The lack of RPE atrophy suggests that viable photoreceptors are preserved even at late stages of the disease,[4] but it is not clear whether S-cones and rods are more likely to remain viable than L- and M-cones. Possibly, disease-related deficits are mainly restricted to the fovea where S-cones are absent. The loss of S-cone- and rod-driven sensitivities in the oldest patient in the cohort is likely related to cataract and other age-related changes in the visual system.

Rods

The RP1L1 gene is expressed in cones and rods.[9] Using chromatic perimetry, Miyake et al. have measured cone and rod absolute thresholds in 12 patients with OMD and have found normal dark-adapted responses in 6 younger patients, and borderline or abnormal sensitivities in the 6 older patients.[7] However, the silent substitution technique offers superior quality of isolation of the different photoreceptor types than chromatic adaptation[19] or dark adaptation.[42] In the present study, we have found preserved rod-driven sensitivities at frequencies between 8 and 12 Hz. Although we cannot fully exclude perception of rod-driven stimuli outside the test field through stray light, we are confident that our data demonstrate that rod-driven function at intermediate frequencies is not severely affected.

The Low-Pass and Band-Pass Groups

Genetically, our cohort was homogeneous. Phenotypically, however, we observed two distinct subgroups with different temporal patterns of the rod-driven (and the L-cone-driven) tCS loss functions. The external validity of this grouping was supported by statistically significant differences in visual acuity, refraction, pattern of perimetric loss, and by tendency for different patterns in the EZ/RPE ratios in the OCT reflectivity profiles. This indicates that OMD disease can manifest itself in different ways. This notion is reinforced when considering that the low-pass group was intrinsically relatively heterogeneous.

Other authors have also found different functional[3,14] and structural phenotypes[4,13,15] in patients with OMD despite a very homogeneous genotype (dominance of patients with the heterozygous R45W mutation). As in our study, it was usually not possible to discriminate different stages in disease progression from distinct phenotypes, due to the studies' cross-sectional nature.[4] Although, the clinical parameters suggest a more progressed disease stage in the low-pass group, this group displayed better rod sensitivities at low temporal frequencies.

It is unlikely that the frequency-dependent differences between groups are caused by different temporal properties of the photoreceptors because this would result in similar frequency dependency of the sensitivities driven by single photoreceptor types. Temporal resolution at the photoreceptor level is much higher than the observed psychophysical temporal resolution, and tCSFs reflect activity of postreceptoral processes that act as filters, transmitting certain frequencies better than others depending on the pathways and adaptation,[43] resulting in a low-pass or a band-pass pattern. Thus, distinct tCSFs indicate differences in the postreceptoral pathways underlying the psychophysical task. Furthermore, earlier studies support the notion that the observed effects are post-receptoral.[22,44] In the band-pass group, rod-driven sensitivities were impaired only at low temporal frequencies, where perception is possibly mediated by the cone-opponent system through gap junctions between rods and cones.[45] Although rod signals are primarily transmitted to MC cells in the macaque, there was also input to PC cells in primates.[46,47] We hypothesize that the band-pass pattern is caused by loss of sensitivities at low temporal frequencies due to disruption of the (parvocellular) red-green opponency system. This notion is supported by the band-pass pattern in the L-cone-driven tCS deviation functions in the band-pass group.

In healthy trichromatic subjects, L- and M-cone-driven contrast sensitivities are very similar at low temporal frequencies, where perception is mediated by the parvocellular red-green opponency system, that receives balanced inputs from L- and M-cones.[21,22,48,49] On the other hand, L-cone-driven sensitivities are higher at higher temporal frequencies, when perception is mediated by the magnocellular luminance system,[21,22,50] because most subjects have more L-cone than M-cones.[48] Although we accounted for these differences by calculating tCS deviations, a relative sparsity and the concurrent absence of signal redundancy might be associated with a more rapid decline in function when further photoreceptors are lost.

Differences in Clinical Parameters Between Groups

Patients in the low-pass group were more myopic than in the band-pass group. Because refractive errors were corrected with glasses, the image of the test field on the retina was smaller. In the patients with the most pronounced myopia, the image was approximately 20% smaller than in the emmetropic patients (vertex distance of 12 mm), but, on average, it was only approximately 8% smaller. Refraction affects perimetry in a similar manner and, in the low-pass group, would lead to: (1) lower perimetric sensitivities because of the smaller stimulus size, and (2) seemingly larger area of the central scotoma due to the smaller visual field as a whole. This was indeed observed in our cohort (see Fig. 5). However, it seems unlikely that this retinal image size effect explains the differences in the tCS deviation curves, because the stimulus of the LED stimulator would fall on more severely affected and more parvocellularly dominated retina in the low-pass group, but we observed poorer parvocellularly driven sensitivities in the band-pass group instead.

Alternatively, development of myopia might modify photoreceptor damage in patients with OMD. To our knowledge, the effect of myopia on visual function in patients with RP1L1 (with refractive correction) has not yet been systematically investigated.

The analysis of the OCTs is also affected by myopic changes. First, the ROIs were spaced 100 µm apart, which corresponds to 1 degree in an emmetropic eye. However, in a

myopic eye, this would correspond to smaller visual angles. Second, the ORA software does not allow to rotate regions of interest (ROIs), leading to underestimation of EZ reflectivities in eyes with a strong macular curvature, because the reflective bands now coincide with different horizontal bands. This may influence the EZ/RPE ratio. Altogether, estimating the effect of refraction on analysis of the OCT band reflectivities is difficult without axial length measurements. Therefore, the (statistically not significant) differences in OCT reflectivities between groups must be appraised critically and should be more thoroughly investigated in future studies.

In conclusion, direct comparison of structure and function may not be straightforward. Furthermore, our analysis of EZ/RPE ratios depends on the assumption that RPE reflectivity is not altered in OMD, because we use RPE as reference. However, no visible RPE alterations were observed and the RPE has been used for normalization of OCT reflectivities in one other study on OMD.[13] Finally, it is not clear whether EZ layer reflectivity always corresponds to photoreceptor viability.[51] This can also be seen in the relatively low foveal EZ reflectivities in the normal subjects.

Pathophysiological Interpretation

The pathological mechanism behind RP1L1-related OMD is not fully elucidated. Clinical data suggest that changes are limited to the macula and that mostly L- and M-cone-related functions like visual acuity and color discrimination are affected. This agrees with the results of the clinical data and the photoreceptor-specific tCS functions in the present study. It also agrees with the strong changes in the AO images found by Nakanishi and coworkers.[6]

L- and M-cone-driven stimuli are detected by the parvocellular (red-green opponent) pathway at low temporal frequencies and by the magnocellular (luminance) pathway at high temporal frequencies.[22] Our data strongly suggests that the parvocellular system is selectively affected in the band-pass group but not in the low-pass group.

This conclusion would infer that the rod-driven tCFs are mediated by the parvocellular pathway at low temporal frequencies. Under high scotopic conditions, rod signals are transmitted via rod bipolar cells and rod-driven temporal contrast sensitivities have a band-pass-shaped dependency on temporal frequency with highest sensitivities at intermediate temporal frequencies around 8 Hz. In healthy subjects, however, mesopic temporal contrast sensitivities are relatively high at low temporal frequencies. Under these conditions, rod-driven responses also induce color perception, an effect that has been studied in detail by Cao et al.[25] Although, we cannot fully rule out cone intrusion in our data, the observed changes in rod-driven sensitivities with changing light levels[35] argues against that and might suggest perception via gap junctions between rods and cones. When cones are lost, rod-driven sensitivities at low temporal frequencies mediated by these gap junctions would be affected, resulting in a band-pass pattern.

Strength and Limitations

The robust, reliable, and well-validated quality of photoreceptor isolation due to the silent substitution technique is one strength of our study. Furthermore, linear mixed effects models[36,37] allowed the analysis of the data by considering both fixed and random effects. The small sample size is a clear limitation of our study, although it is somewhat mitigated by the fact that comparisons between photoreceptor subtypes (primary outcome) are performed intra-individually ("paired data") which reduces the negative effects of the large interindividual variability.

A further limitation is the lack of axial length measurements to account for alterations of the retinal image size by correcting lenses. Due to the cross-sectional nature of the study, we also cannot discriminate effects of disease progression over time from phenotypic differences in our groups. Furthermore, we did not have a direct age-matched control group. Although this would have been ideal, measurements are time-consuming, and it is not always easy to recruit aged-matched normal subjects for the older patients. Therefore, we have developed a model for age-dependent normative data, an approach that is also used in standard-automated perimetry.[28]

In the present study, it was difficult to rule out X-chromosomal color vision defects due to the magnitude of the acquired color vision defects. Patients had difficulties performing the anomaloscope examination, which would be the only test that yields direct information about the spectral sensitivities of the L- and M-cone opsins. From earlier experience, we hypothesized that the tCS measurements themselves might allow identification of dichromacy, but one patient with characteristics of dichromacy in this cohort was found to have an almost normal Panel-D15 more than 10 years ago.

Impact for Clinicians

Our study underscores the power of psychophysical tests in OMD. Our data show that there was selective impairment of the L- and M-cone-driven functions, that S-cone-driven function was impaired to a lesser degree and that rod function was normal. The terms "L-cone-driven function" must be used instead of "L-cone function" because it is not always possible to draw direct conclusions on photoreceptor function from psychophysical data.

In the process, we have also identified two subgroups which differ strongly in visual function and show very different patterns in photoreceptor-specific contrast sensitivity functions. Although there is also a tendency toward structural differences between these groups, these are subtle in comparison to the functional test, and it is difficult two discriminate the two groups on the basis of the OCT. This warrants further research in the future.

Our method is currently not suited for clinical application, because photoreceptor-specific temporal contrast sensitivity measurements are reserved for highly specialized vision research laboratories, where functional test based on the silent substitution technique are a valuable tool for investigating the mechanisms of retinal function in healthy subjects and in patients with retinal diseases.

Outlook

In the future, clinical tests based on the silent substitution paradigm should be developed (e.g. perimetry with rod and cone isolating stimuli). Patients with OMD would be a good cohort for validation of such new tests, because they are genetically very homogeneous, retain central fixation and a minimal visual acuity, and have clear L- and M-cone specific effects.

Conclusions

Photoreceptor-specific temporal contrast sensitivity functions demonstrated selective damage to L- and M-cone signals in patients with OMD and sparing of the rods. In a subgroup, the parvocellular red-green-opponency system was predominantly affected. This ("band-pass") group was relatively homogeneous and had retained a better central function compared with the other ("low-pass") group. Sophisticated functional tests based on the silent substitution mechanism are useful for investigating diseases like OMD.

Acknowledgments

Supported by Deutsche Forschungsgemeinschaft (German Research Council) Priority Program SPP2127: HU2340/1-2 to C.H. and KR1317/16-1 to J.K. and STI 727/1-1 to Ka.S. and M.K.

Disclosure: **C. Huchzermeyer**, None; **J. Fars**, None; **J. Kremers**, None; **L. Kühlewein**, None; **M. Kempf**, None; **S. Ott**, None; **K. Stingl**, None; **K. Stingl**, None

References

1. Zobor D, Zobor G, Hipp S, et al. Phenotype variations caused by mutations in the RP1L1 gene in a large mainly German cohort. *Invest Ophthalmol Vis Sci*. 2018;59(7):3041–3052.
2. Huchzermeyer C, Fars J, Stöhr H, Kremers J. [New techniques for quantification of color vision in disorders of cone function : Cambridge color test and photoreceptor-specific temporal contrast sensitivity in patients with heterozygous RP1L1 and RPGR mutations]. *Ophthalmol Z Dtsch Ophthalmol Ges*. 2021;118(2):144–153.
3. Ahn SJ, Yang L, Tsunoda K, et al. Visual field characteristics in East Asian patients with occult macular dystrophy (Miyake disease): EAOMD report no. 3. *Invest Ophthalmol Vis Sci*. 2022;63(1):12.
4. Nakamura N, Tsunoda K, Mizuno Y, et al. Clinical stages of occult macular dystrophy based on optical coherence tomographic findings. *Invest Ophthalmol Vis Sci*. 2019;60(14):4691–4700.
5. Chen CJ, Scholl HPN, Birch DG, Iwata T, Miller NR, Goldberg MF. Characterizing the phenotype and genotype of a family with occult macular dystrophy. *Arch Ophthalmol Chic Ill 1960*. 2012;130(12):1554–1559.
6. Nakanishi A, Ueno S, Kawano K, et al. Pathologic changes of cone photoreceptors in eyes with occult macular dystrophy. *Invest Ophthalmol Vis Sci*. 2015;56(12):7243–7249.
7. Miyake Y, Horiguchi M, Tomita N, et al. Occult macular dystrophy. *Am J Ophthalmol*. 1996;122(5):644–653.
8. Akahori M, Tsunoda K, Miyake Y, et al. Dominant mutations in RP1L1 are responsible for occult macular dystrophy. *Am J Hum Genet*. 2010;87(3):424–429.
9. Noel NCL, MacDonald IM. RP1L1 and inherited photoreceptor disease: a review. *Surv Ophthalmol*. 2020;65(6):725–739.
10. Yamashita T, Liu J, Gao J, et al. Essential and synergistic roles of RP1 and RP1L1 in rod photoreceptor axoneme and retinitis pigmentosa. *J Neurosci Off J Soc Neurosci*. 2009;29(31):9748–9760.
11. Conte I, Lestingi M, den Hollander A, et al. Identification and characterisation of the retinitis pigmentosa 1-like1 gene (RP1L1): a novel candidate for retinal degenerations. *Eur J Hum Genet EJHG*. 2003;11(2):155–162.
12. Davidson AE, Sergouniotis PI, Mackay DS, et al. RP1L1 variants are associated with a spectrum of inherited retinal diseases including retinitis pigmentosa and occult macular dystrophy. *Hum Mutat*. 2013;34(3):506–514.
13. Kato Y, Hanazono G, Fujinami K, et al. Parafoveal photoreceptor abnormalities in asymptomatic patients with RP1L1 mutations in families with occult macular dystrophy. *Invest Ophthalmol Vis Sci*. 2017;58(14):6020–6029.
14. Yang L, Joo K, Tsunoda K, et al. Spatial functional characteristics of East Asian patients with occult macular dystrophy (Miyake disease); EAOMD report no. 2. *Am J Ophthalmol*. 2021;221:169–180.
15. Fujinami K, Yang L, Joo K, et al. Clinical and genetic characteristics of East Asian patients with occult macular dystrophy (Miyake disease): East Asia Occult Macular Dystrophy Studies Report Number 1. *Ophthalmology*. 2019;126(10):1432–1444.
16. Estevez O, Spekreijse H. The "silent substitution" method in visual research. *Vision Res*. 1982;22(6):681–691.
17. Donner KO, Rushton WAH. Retinal stimulation by light substitution. *J Physiol*. 1959;149(2):288–302.
18. Huchzermeyer CRH, Mardin CY, Lämmer R, Kremers JJ. Combining L- and M-cone-isolating stimuli to measure parvo- and magnocellular function in normal subjects and glaucoma patients. *Invest Ophthalmol Vis Sci*. 2019;60(9):2447.
19. Kremers J. The assessment of L- and M-cone specific electroretinographical signals in the normal and abnormal human retina. *Prog Retin Eye Res*. 2003;22(5):579–605.
20. Shapiro AG, Pokorny J, Smith VC. Cone-rod receptor spaces with illustrations that use CRT phosphor and light-emitting-diode spectra. *J Opt Soc Am A Opt Image Sci Vis*. 1996;13(12):2319–2328.
21. Huchzermeyer C, Kremers J. Perifoveal L- and M-cone-driven temporal contrast sensitivities at different retinal illuminances. *J Opt Soc Am A*. 2016;33(10):1989.
22. Smith VC, Pokorny J, Davis M, Yeh T. Mechanisms subserving temporal modulation sensitivity in silent-cone substitution. *J Opt Soc Am A Opt Image Sci Vis*. 1995;12(2):241–249.
23. Sharpe LT, Stockman A. Rod pathways: the importance of seeing nothing. *Trends Neurosci*. 1999;22(11):497–504.
24. Zele AJ, Cao D. Vision under mesopic and scotopic illumination. *Front Psychol*. 2014;5:1594.
25. Cao D, Pokorny J, Smith VC, Zele AJ. Rod contributions to color perception: linear with rod contrast. *Vision Res*. 2008;48(26):2586–2592.
26. Jolly JK, Menghini M, Johal PA, Buckley TMW, Bridge H, Maclaren RE. Inner retinal thickening affects microperimetry thresholds in the presence of photoreceptor thinning in patients with RPGR retinitis pigmentosa. *Br J Ophthalmol*. 2022;106:256–261.
27. Pokorny J, Smithson H, Quinlan J. Photostimulator allowing independent control of rods and the three cone types. *Vis Neurosci*. 2004;21(3):263–267.
28. Huchzermeyer C, Fars J, Kremers J. Photoreceptor-specific loss of perifoveal temporal contrast sensitivity in retinitis pigmentosa. *Transl Vis Sci Technol*. 2020;9(6):27.
29. Fars J, Pasutto F, Kremers J, Huchzermeyer C. Perifoveal cone- and rod-mediated temporal contrast sensitivities in Stargardt disease/fundus flavimaculatus. *Invest Ophthalmol Vis Sci*. 2021;62(14):24.
30. Marín-Franch I, Swanson WH. The visualFields package: a tool for analysis and visualization of visual fields. *J Vis*. 2013;13(4).
31. R Core Team. *R: a Language and Environment for Statistical Computing*. R Foundation for Statistical Computing; 2022. Available at: https://www.R-project.org/.
32. Wilk MA, Wilk BM, Langlo CS, Cooper RF, Carroll J. Evaluating outer segment length as a surrogate measure of peak foveal cone density. *Vision Res*. 2017;130:57–66.

Investigative Ophthalmology & Visual Science

33. Vingrys AJ, King-Smith PE. A quantitative scoring technique for panel tests of color vision. *Invest Ophthalmol Vis Sci*. 1988;29(1):50–63.
34. Puts MJH, Pokorny J, Quinlan J, Glennie L. Audiophile hardware in vision science; the soundcard as a digital to analog converter. *J Neurosci Methods*. 2005;142(1):77–81.
35. Huchzermeyer C, Kremers J. Perifoveal S-cone and rod-driven temporal contrast sensitivities at different retinal illuminances. *J Opt Soc Am A*. 2017;34(2):171.
36. Kuznetsova A, Brockhoff PB, Christensen RHB. lmerTest package: tests in linear mixed effects models. *J Stat Softw*. 2017;82(13):1–26.
37. Knoblauch K, Maloney LT. Modeling in R. In: Knoblauch K, Maloney LT, eds. *Modeling Psychophysical Data in R*. Use R! New York, NY: Springer Publishing; 2012:21–60.
38. Paramei GV. Color discrimination across four life decades assessed by the Cambridge Colour Test. *J Opt Soc Am A Opt Image Sci Vis*. 2012;29(2):A290–A297.
39. Rüfer F, Sauter B, Klettner A, Göbel K, Flammer J, Erb C. Age-corrected reference values for the Heidelberg multicolor anomaloscope. *Graefes Arch Clin Exp Ophthalmol*. 2012;250(9):1267–1273.
40. Huchzermeyer C, Kremers J, Barbur J. Color vision in clinical practice. In: Kremers J, Baraas RC, Marshall NJ, eds. *Human Color Vision*. New York, NY: Springer International Publishing; 2016:269–315.
41. Hood DC, Benimoff NI, Greenstein VC. The response range of the blue-cone pathways: a source of vulnerability to disease. *Invest Ophthalmol Vis Sci*. 1984;25(7):864–867.
42. Maguire J, Parry NRA, Kremers J, Kommanapalli D, Murray IJ, McKeefry DJ. Rod electroretinograms elicited by silent substitution stimuli from the light-adapted human eye. *Transl Vis Sci Technol*. 2016;5(4):13.
43. Conner JD, MacLeod DI. Rod photoreceptors detect rapid flicker. *Science*. 1977;195(4279):698–699.
44. Huchzermeyer C, Martins CMG, Nagy B, et al. Photoreceptor-specific light adaptation of critical flicker frequency in trichromat and dichromat observers. *JOSA A*. 2018;35(4):B106–B113.
45. Cao D, Pokorny J, Smith VC. Matching rod percepts with cone stimuli. *Vision Res*. 2005;45(16):2119–2128.
46. Weiss S, Kremers J, Maurer J. Interaction between rod and cone signals in responses of lateral geniculate neurons in dichromatic marmosets (Callithrix jacchus). *Vis Neurosci*. 1998;15(5):931–943.
47. Lee BB, Smith VC, Pokorny J, Kremers J. Rod inputs to macaque ganglion cells. *Vision Res*. 1997;37(20):2813–2828.
48. Kremers J, Scholl HP, Knau H, Berendschot TT, Usui T, Sharpe LT. L/M cone ratios in human trichromats assessed by psychophysics, electroretinography, and retinal densitometry. *J Opt Soc Am A Opt Image Sci Vis*. 2000;17(3):517–526.
49. Smith VC, Lee BB, Pokorny J, Martin PR, Valberg A. Responses of macaque ganglion cells to the relative phase of heterochromatically modulated lights. *J Physiol*. 1992;458:191–221.
50. Lee BB, Martin PR, Valberg A, Kremers J. Physiological mechanisms underlying psychophysical sensitivity to combined luminance and chromatic modulation. *J Opt Soc Am A*. 1993;10(6):1403–1412.
51. Lee KE, Heitkotter H, Carroll J. Challenges associated with ellipsoid zone intensity measurements using optical coherence tomography. *Transl Vis Sci Technol*. 2021;10(12):27.

Investigative Ophthalmology & Visual Science